Int. J. Nano Dimens., 13 (1): 54-70, Winter 2022

ORIGINAL ARTICLE

The effect of magnetic field on buckling and nonlinear vibrations of Graphene nanosheets based on nonlocal elasticity theory

Tayyeb Pourreza[1], Ali Alijani[1,], Vahid Arab Maleki[1,2], Admin Kazemi[1]*

[1] *Department of Mechanical Engineering, Bandar Anzali Branch, Islamic Azad University, Bandar Anzali, Iran*

[2] *Department of Mechanical Engineering, University of Tabriz, Tabriz, Iran*

Received 15 June 2021; revised 21 July 2021; accepted 04 August 2021; available online 10 August 2021

Abstract

In this paper, the buckling behavior and nonlinear vibrations of graphene nanosheets in the magnetic field are studied analytically. By considering mechanical and magnetic interactions, new relationships have been proposed for the forces exerted by the magnetic field. The nonlinear governing equation is derived using Kirchhoff's thin plate theory in conjunction with the nonlocal strain gradient theory of elasticity and von Karman's nonlinear strain-displacement relation. The nonlinear governing equation is discretized using the Galerkin method. According to the method of multiple scales, the approximate analytical solutions are extracted. For the three considered boundary conditions, nonlinear natural frequencies and amplitude-frequency curves are computed for different values of magnetic field and nonlocal parameters. The results show that increasing the nonlocal parameter and applying a magnetic field reduces the flexural stiffness and increases the in-plate compressive force which results in reducing the natural frequency. In addition, excessive magnification of the magnetic field causes static buckling. The value of the critical magnetic field is highly dependent on the type of boundary conditions.

Keywords: *Buckling; Graphene Nanosheets; Magnetic Field; Natural Frequency; Nonlinear Vibrations.*

How to cite this article

Pourreza T., Alijani A., Arab Maleki V., Kazemi A. The effect of magnetic field on buckling and nonlinear vibrations of Graphene nanosheets based on nonlocal elasticity theory. Int. J. Nano Dimens., 2022; 13(1): 54-70.

INTRODUCTION

With the development of nanotechnology, application of the nanoparticles has been increased in many structures due to their unique properties [1-3]. Nanoparticles such as Al_2O_3 [4-6], TiO_2 [7, 8], Cu [9, 10], SiO_2 [11], CNT [12, 13], and graphene nanosheets are one of the essential components in industrial applications which expose them to work under the magnetic medium of varying mechanical and magnetohydrodynamic loads [14-16]. Due to their considerable mechanical properties as well as very high natural frequencies (in the range of above GHz), these nanosheets have found a wide range of applications in the mechanical nanosensors as one of the most important nano-electromechanical systems (NEMS). Caused by the difficulty of performing experimental tests on the NEMS, the use of the analytical models and continuum mechanics to study the dynamic behavior of these systems has been considered by many researchers [17].

As it was previously mentioned, graphene nanosheets possess unique properties including high hardness, high mechanical strength, very high electrical and thermal conductivity, flexibility, and magnetic properties. Due to these properties, graphene has been widely used in various fields of human life such as agriculture, medicine, electronics, transportation, defense, and so on. Many studies have been conducted to investigate the vibration and buckling behavior of graphene sheets [18-21]. Aghababaei and Reddy [22] rewrote the third-order shear deformation theory

* Corresponding Author Email: *alijani@iaubanz.ac.ir*

of plates using Eringen's linear theory of nonlocal elasticity, which could simultaneously apply small-scale effects and quadratic variables of shear strain and thus shear stress in plate thickness. Murmu and Pradhan [23] implemented Eringen's linear theory of nonlocal elasticity to study the vibration response of monolayer graphene sheets. Ebrahimi and Barati [24] studied the vibrational behavior of graphene sheets located on an elastic foundation under the influence of in-plane magnetic fields using the theory of nonlocal strains. Jalali and Ghorbanpour [25] studied the nonlocal vibration of double-walled graphene nanosheets, which are bonded together by an elastic medium and affected by a magnetic field under different boundary conditions. Murmu *et al.* [26] studied the effect of magnetic fields on the transverse vibration behavior of monolayer graphene nanosheets located on an elastic foundation using the improved nonlocal elasticity theory. In their study, the in-plane magnetic field was applied to the graphene nanosheets. The intensity of the magnetic field was calculated using Lorentz equations, and the effect of different magnetic field parameters on the behavior of the system was investigated. Using the differential quadrature method, Esmaeili and Biglari [27] solved the governing equation on the lateral vibration of a single-layer graphene nanosheet under the influence of an in-plane two-dimensional magnetic field for different boundary conditions. In their study, the governing equation on the vibration of the nanosheet was derived using nonlocal theory and considering the Lorentz magnetic force. Farajpour *et al.* [28] studied the buckling of circular graphene nanosheets placed on the Winkler-Pasternak elastic foundation using the non-local elasticity theory. Samaei *et al.* [29] used the Levy solution model to investigate the bending response of monolayer graphene sheets under the temperature field as the external mechanical load. They obtained the differential equations governing the thermomechanical response based on Eringen's equations of non-local elasticity by combining the two-variable sheet theory and using the Mindlin plane theory. Pradhan [30] discussed the buckling behavior of monolayer rectangular graphene sheets using the nonlinear elastic rectangular sheet model and the higher-order shear deformations theory, taking into account quantum effects.

Allahyari *et al.* [31] employed a multiple-scale perturbation method to analyze nonlinear free vibration of graphene nanoplate incorporating surface effects. Eringen's nonlocal theory as well as the surface elasticity theory of Gurtin and Murdoch is used to consider small scale effect. Rong *et al.* [32] extracted the equations of the buckling of orthotropic graphene nanosheets using Eringen's nonlocal theory and solved these equations using the finite difference method. They investigated the buckling of the rectangular nanosheets under uniform and non-uniform linear in-plane loadings. The results of their study show that the critical buckling load without a nonlocal dimension is always less than or equal to the corresponding classical buckling critical load. Nonlinear forced vibrations of initially curved rectangular single-layer graphene sheets were investigated by Saadatmand *et al.* [33]. Mortazavi *et al.* [34] used classical molecular dynamics simulations to explore the thermal conductivity and mechanical response of two main structures.

Among all of the mentioned properties, graphene is an application in many applications such as energy storage, sensors, electronics, graphene field-effect transistors, and more. Magnetic force microscopy signals have recently been detected from whole pieces of mechanically exfoliated graphene nanosheets, and magnetism of the two nanomaterials was claimed based on these observations. In these systems graphene nanosheets are under different tip voltages, electrical current, and magnetic fields [35]. As an example, Dhakal and Rai [36] studied magnetic field control of current through model graphene nanosheet junctions within the framework of the tight-binding approximation.

Based on the available literature, the free and forced vibrations of graphene nanosheets have been considered by researchers from different aspects [37]. Despite the increased knowledge about graphene nanosheets applications over the last two decades, a few attentions has been paid to the possible effect of electromagnetic force on the vibrational behavior of nanostructures. Also, a study on the vibration behavior and nonlinear buckling of graphene nanosheets affected by electromagnetic charges is not found in the literature. Accordingly, in this research, the vibration and buckling behavior of graphene nanosheets in the presence of electromagnetic charges are studied using nonlocal theory. To apply more realistic assumptions, taking into account the effects of magnetic interactions and

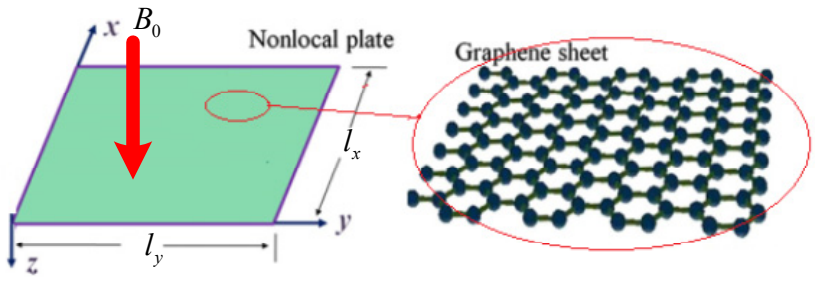

Fig. 1. Mathematical model of graphene nanosheet located in the magnetic field.

the created displacement fields, new relationships are proposed for electromagnetic interaction forces. The electromagnetic force and momentum resultants are calculated using Maxwell's equations. Then, using Newton's second law, the governing equations of motion are derived. Finally, after discretizing the equations using the Galerkin method, the nonlinear equation is solved using the multiple time scales method. The effects of geometric and physical parameters on changes in natural frequencies, buckling loads, and amplitude-frequency curves of the graphene nanosheets are studied.

MATERIALS AND METHODS

As it can be seen in Fig. 1, a rectangle graphene nanosheet with length l_x, width l_y and thickness *h* is considered According to the nonlocal strain theory, the nonlocal constitutive equation is expressed as follows [18]:

$$\left(1-\mu\nabla^2\right)\sigma^{nl}=C:\varepsilon,\quad \mu=(e_0a)^2 \tag{1}$$

in which C, ε and σ^{nl} represents the fourth-order elasticity tensor, strain and nonlocal stress tensor respectively. μ is the scale parameter, e_0 is constant appropriate to each material and *a* is internal characteristic length. ∇^2 is the Laplacian operator which is expressed as follows:

$$\nabla^2=\frac{\partial^2}{\partial x^2}+\frac{\partial^2}{\partial y^2} \tag{2}$$

Using Eq. (1), two-dimensional nonlocal constitutive relationships can be expressed as follows:

$$\sigma_x-(e_0a)^2\left(\frac{\partial^2\sigma_x}{\partial x^2}+\frac{\partial^2\sigma_x}{\partial y^2}\right)=\frac{E}{1-\nu^2}\left(\varepsilon_x+\nu\varepsilon_y\right) \tag{3}$$

$$\sigma_y-(e_0a)^2\left(\frac{\partial^2\sigma_y}{\partial x^2}+\frac{\partial^2\sigma_y}{\partial y^2}\right)=\frac{E}{1-\nu^2}\left(\varepsilon_y+\nu\varepsilon_x\right) \tag{4}$$

$$\tau_{xy}-(e_0a)^2\left(\frac{\partial^2\tau_{xy}}{\partial x^2}+\frac{\partial^2\tau_{xy}}{\partial y^2}\right)=G\varepsilon_{xy} \tag{5}$$

where E, G and ν represent Young's modulus, shear modulus and Poisson's ratio, respectively.

Using Kirchhoff's theory of plates, the displacement fields are expressed as follows [22]:

$$\begin{aligned} u_1&=u(x,y,t)-z\frac{\partial w}{\partial x},\\ u_2&=v(x,y,t)-z\frac{\partial w}{\partial y},\\ u_3&=w(x,y,t)\end{aligned} \tag{6}$$

where u_1 and u_2 are the in-plane displacements of each arbitrary point of the plate in the *x* and *y* directions, also u_3 is the transverse displacement of the plate along the *z*-axis. u and v are the displacement of the mid-plane of the plate.

$$\boldsymbol{\varepsilon}=\boldsymbol{\varepsilon}_0+z\boldsymbol{\kappa} \tag{7}$$

where $\boldsymbol{\varepsilon}$ is the strain at any point, $\boldsymbol{\varepsilon}_0$ and $\boldsymbol{\kappa}$ represents t+he nonlinear strain vector of the neutral axis and the curvature vector, respectively. Since the nonlinear vibration is due to the large deformations, the von-Karman strain-displacement relations are used as [22]:

$$\boldsymbol{\varepsilon}_0=\left\{\frac{\partial u_0}{\partial x}+\frac{1}{2}\left(\frac{\partial w}{\partial x}\right)^2,\frac{\partial v_0}{\partial y}+\frac{1}{2}\left(\frac{\partial w}{\partial y}\right)^2,\frac{\partial u_0}{\partial y}+\frac{\partial v_0}{\partial x}+\frac{\partial w}{\partial x}\frac{\partial w}{\partial y}\right\}^T \tag{8}$$

$$\boldsymbol{\kappa}=\left\{-\frac{\partial^2 w}{\partial x^2},-\frac{\partial^2 w}{\partial y^2},-2\frac{\partial^2 w}{\partial x\partial y}\right\} \quad (9)$$

The nonlocal stress resultant of the nanoplate can be expressed as follows:

$$\begin{aligned} M_{xx}&=\int_{-h/2}^{h/2} z\sigma_{xx}^{nl}dz,\\ M_{yy}&=\int_{-h/2}^{h/2} z\sigma_{yy}^{nl}dz,\\ M_{xy}&=\int_{-h/2}^{h/2} z\sigma_{xy}^{nl}dz, \end{aligned} \quad (10)$$

Taking into account the nonlocal theory and external forces, as well as disregarding the in-plane inertial forces, the transverse equilibrium equation of the graphene nanosheet is obtained as follows:

$$\begin{aligned} &\frac{\partial^2 M_{xx}}{\partial x^2}+2\frac{\partial^2 M_{xy}}{\partial x\partial y}+\frac{\partial^2 M_{yy}}{\partial y^2}+\\ &\frac{\partial}{\partial x}\left(N_{xx}\frac{\partial w}{\partial x}+N_{xy}\frac{\partial w}{\partial y}\right)+\frac{\partial}{\partial y}\left(N_{y}\frac{\partial w}{\partial y}+N_{xy}\frac{\partial w}{\partial x}\right)\\ &+F_z(x,y,t)+q(t)=m_0\frac{\partial^2 w}{\partial t^2}-m_2\left(\frac{\partial^4 w}{\partial x^2\partial t^2}+\frac{\partial^4 w}{\partial y^2\partial t^2}\right) \end{aligned} \quad (11)$$

where $m_0=\int_{-h/2}^{h/2}\rho dz$ and $m_2=\int_{-h/2}^{h/2}\rho z^2 dz$ and $F_z(x,y,t)$ is used to show the external forces applied by the magnetic field and mechanical forces. N_x, N_y and N_{xy} represent the resultant forces. M_x, M_y and M_{xy} represent the resultant momentums per unit length along the *x*- and *y*-axes, respectively, and are determined using nonlocal strain theory as follows:

$$\begin{aligned} M_{xx}&=\int_{-h/2}^{h/2} z\sigma_{xx}^{nl}dz,\\ M_{yy}&=\int_{-h/2}^{h/2} z\sigma_{yy}^{nl}dz,\\ M_{xy}&=\int_{-h/2}^{h/2} z\tau_{xy}^{nl}dz \end{aligned} \quad (12)$$

Using Equations (8), (9) and (13), the momentum resultants are obtained as follows:

$$\left(1-\mu\nabla^2\right)M_{xx}=-D\frac{\partial^2 w}{\partial x^2}-\nu D\frac{\partial^2 w}{\partial y^2} \quad (13)$$

$$\left(1-\mu\nabla^2\right)M_{yy}=-D\frac{\partial^2 w}{\partial y^2}-\nu D\frac{\partial^2 w}{\partial x^2} \quad (14)$$

$$\left(1-\mu\nabla^2\right)M_{xy}=-\left(1-\mu\nabla^2\right)M_{yx}=D(1-\nu)\frac{\partial^2 w}{\partial x\partial y} \quad (15)$$

where $D=Eh^3/12\left(1-\nu^2\right)$ is the flexural stiffness of the nanosheet.

By applying the linear operator $1-\mu\nabla^2$ to each side of the equilibrium equation (12) and using the relations (14) - (16), the nonlocal equation of motion of the nanosheet is obtained as follows:

$$\begin{aligned} &D\left(\frac{\partial^4 w}{\partial x^4}+2\frac{\partial^2 w}{\partial x^2\partial y^2}+\frac{\partial^2 w}{\partial y^4}\right)=\\ &-\rho h\left(1-\mu\nabla^2\right)\frac{\partial^2 w}{\partial t^2}+\left(1-\mu\nabla^2\right)F_z(x,y,t) \end{aligned} \quad (16)$$

In-plane membrane forces appear in large deformations of plates. Assume that this element is subject to the in-plane per length forces of N_i, so the equilibrium equations along the x and y axes are obtained based on Fig. 2 as follows:

$$\frac{\partial N_x}{\partial x}+\frac{\partial N_{xy}}{\partial y}=0 \quad (17)$$

$$\frac{\partial N_y}{\partial y}+\frac{\partial N_{xy}}{\partial x}=0 \quad (18)$$

It has been shown that the effect of perpendicular membrane forces on the transverse deflection of the nanosheet can be obtained using the equilibrium equation in the z-direction [38-40]. According to the force equilibrium of the element shown in Fig. 3 and ignoring the high-power terms, the total membrane force in the vertical direction is obtained as follows:

$$F_z(x,y,t)=N_x\frac{\partial^2 w}{\partial x^2}+N_y\frac{\partial^2 w}{\partial y^2}+2N_{xy}\frac{\partial^2 w}{\partial x\partial y} \quad (19)$$

Adding the transverse force obtained in the above relation to Equation (17) we have:

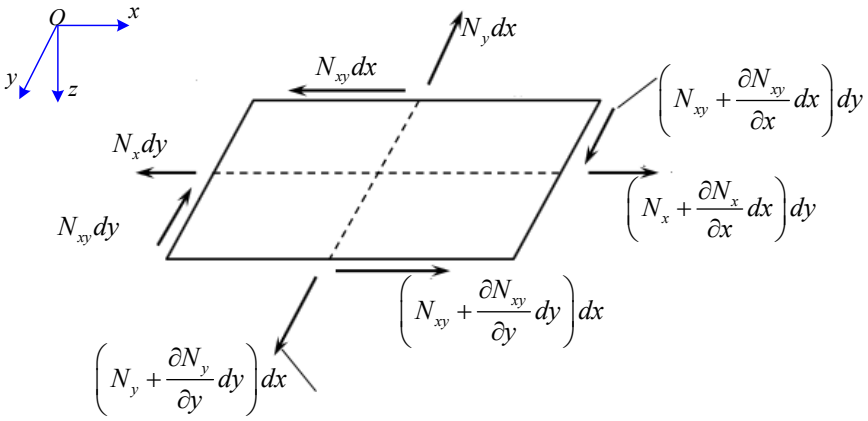

Fig. 2. In-plane forces in a graphene element.

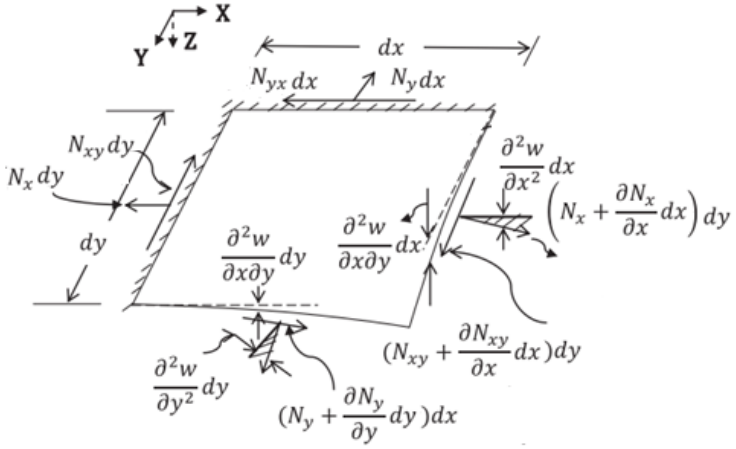

Fig. 3. The free-body diagram of nanoplate element.

$$D\left(\frac{\partial^4 w}{\partial x^4} + 2\frac{\partial^2 w}{\partial x^2 \partial y^2} + \frac{\partial^2 w}{\partial y^4}\right) = -\rho h\left(1-\mu\nabla^2\right)\frac{\partial^2 w}{\partial t^2} + \left(1-\mu\nabla^2\right)\left[N_x \frac{\partial^2 w}{\partial x^2} + N_y \frac{\partial^2 w}{\partial y^2} + 2N_{xy}\frac{\partial^2 w}{\partial x \partial y}\right] + \left(1-\mu\nabla^2\right)P_z \quad (20)$$

Equation (21) represents the differential equation governing the vibrations of graphene nanosheets exposed to a magnetic field. In Equation (20), the nonlocal resultant stresses of the nanosheet can be expressed as:

$$N_{xx} = \int_{-h/2}^{h/2} \sigma_{xx}^{nl} dz,\ N_{yy} = \int_{-h/2}^{h/2} \sigma_{yy}^{nl} dz,\ N_{xy} = \int_{-h/2}^{h/2} \sigma_{xy}^{nl} dz \quad (21)$$

Using Equations (3) - (5), the above equations can be simplified as follows:

$$\begin{aligned}
\left(1-\mu\nabla^2\right)N_{xx} &= \frac{Eh}{1-\nu^2}\left(\varepsilon_x + \nu\varepsilon_y\right)\\
\left(1-\mu\nabla^2\right)N_{yy} &= \frac{Eh}{1-\nu^2}\left(\varepsilon_y + \nu\varepsilon_x\right)\\
\left(1-\mu\nabla^2\right)N_{xy} &= Gh\varepsilon_{xy}
\end{aligned} \quad (22)$$

Finally, by using Equation (8) and ignoring the displacement fields in the *x*- and *y*- directions, the in-plane forces are obtained as:

$$\begin{aligned}
\left(1-\mu\nabla^2\right)N_{xx} &= \frac{Eh}{1-\nu^2}\left(\left(\frac{\partial w}{\partial x}\right)^2 + \nu\left(\frac{\partial w}{\partial y}\right)^2\right)\\
\left(1-\mu\nabla^2\right)N_{yy} &= \frac{1}{2}\frac{Eh}{1-\nu^2}\left(\left(\frac{\partial w}{\partial y}\right)^2 + \nu\left(\frac{\partial w}{\partial x}\right)^2\right)\\
\left(1-\mu\nabla^2\right)N_{xy} &= Gh\frac{\partial w}{\partial x}\frac{\partial w}{\partial y}
\end{aligned} \quad (23)$$

Because graphene nanosheets have high electrical conductivity properties, so according to the Maxwell equations, the electromagnetic equations governing the system will be as follows [41]:

$$\nabla \cdot \mathbf{B} = 0,\ \nabla \times \mathbf{H} = \mathbf{J}_f,\ \ \mathbf{M} = \chi_m \mathbf{H},\ \ \mathbf{H} = \frac{1}{\mu_0}\mathbf{B} \quad (24)$$

where $\mathbf{B}$, $\mathbf{H}$, $\mathbf{J}_f$, $\mathbf{M}$ and ∇ are the magnetic field intensity, the magnetic flux density, the density-current vector, the magnetization vector, and the gradient operator, respectively.

Considering the magnetic field perpendicular to the plate and the absence of electrical current, $\mathbf{B} = (0, 0, B_0)$ the electromagnetic forces and momentums can be obtained as follows. The details of their extraction are given in the previous work of the authors [41].

$$\frac{\partial C_y}{\partial x} = -\frac{hB_0^2\left(\chi_m - 1\right)}{2\mu_0}\frac{\partial^2 w}{\partial x^2} \quad (25)$$

$$P_z^{EMf}(x,y,t) = \left(1-\mu\nabla^2\right)\left[T_z^{EM} - T_x^{EM}\frac{\partial w}{\partial x} - T_y^{EM}\frac{\partial w}{\partial y}\right] \quad (26)$$

in which

$$T_z^{EM} = \frac{B_0^2}{2\mu_0\left(1+\chi_m\right)}\left[\left(10\chi_m^2 - 2\chi_m - 1\right)\left(\frac{\partial w}{\partial x}\right)^2 + \left(4\chi_m + 2\right)\frac{\partial w}{\partial x}\right]$$
$$T_x^{EM} = 0,\ \ T_y^{EM} = \frac{B_0^2\left(\chi_m - 1\right)}{\mu_0}\frac{\partial w}{\partial y} \quad (27)$$

Non-dimensional equation governing the transverse vibrations of graphene nanosheet located in the magnetic field

Assuming that the system is under the external harmonic force of $P_z^M = P_0 \sin \omega t$ and has structural damping of c, and total applied load expressed as $P_z(x,y,t) = P_z^M + P_z^{EMm} + P_z^{EMf}$. Substituting Equations (23) and (25)-(27) in Equation (20) the governing equation of transverse vibration of the graphene nanosheet located in the magnetic field is obtained as follows:

$$D\left(\frac{\partial^4 w}{\partial x^4} + 2\frac{\partial^4 w}{\partial x^2 \partial y^2} + \frac{\partial^4 w}{\partial y^4}\right) + c\frac{\partial w}{\partial t} + \rho h\left(1-\mu\nabla^2\right)\frac{\partial^2 w}{\partial t^2}$$
$$= -\left(1-\mu\nabla^2\right)\frac{hB_0^2\left(\chi_m - 1\right)}{2\mu_0}\frac{\partial^2 w}{\partial y^2}$$
$$+\left(1-\mu\nabla^2\right)\frac{B_0^2}{2\mu_0\left(1+\chi_m\right)}\left[\left(10\chi_m^2 - 2\chi_m - 1\right)\left(\frac{\partial w}{\partial x}\right)^2 + \left(4\chi_m + 2\right)\frac{\partial w}{\partial x}\right] \quad (28)$$
$$+2Gh\frac{\partial^2 w}{\partial x \partial y}\frac{\partial w}{\partial x}\frac{\partial w}{\partial y} - \left(1-\mu\nabla^2\right)\frac{B_0^2\left(\chi_m - 1\right)}{\mu_0}\left(\frac{\partial w}{\partial y}\right)^2 + P_0 \sin \omega t$$

where the left-hand side the first term is the flexural stiffness, the second term is damping, and the third term is the inertia force. On the right-hand side, the resultants magnetic force and mechanical external force are observed.

If the non-dimensional variables are defined as:

$$\overline{w} = \frac{w}{h},\ \overline{x} = \frac{x}{l_x},\ \overline{y} = \frac{y}{l_x},\ \ \tau = \frac{1}{l_x^2}\sqrt{\frac{D}{\rho h}}t,\ \Omega = l_x^2\sqrt{\frac{\rho h}{D}}\omega,\ \ \overline{P}_0 = \frac{P_0 l_x^4}{Dh}$$
$$S_0 = \frac{\left(\chi_m - 1\right)}{2\mu_0}\frac{hl_x^2}{D},\ S_1 = \frac{\left(10\chi_m^2 - 2\chi_m - 1\right)}{2\mu_0\left(1+\chi_m\right)} \times \frac{hl_x^2}{D},\ \ R_0 = \frac{Gh^3}{D} \quad (29)$$

The equation of motion (28) can be re-written as follows:

$$\left(\frac{\partial^4 \overline{w}}{\partial \overline{x}^4} + 2\frac{\partial^4 \overline{w}}{\partial \overline{x}^2 \partial \overline{y}^2} + \frac{\partial^4 \overline{w}}{\partial \overline{y}^4}\right) + \xi\frac{\partial \overline{w}}{\partial \tau} + \left(1-\mu\nabla^2\right)\frac{\partial^2 \overline{w}}{\partial \tau^2} =$$
$$+\left(\left(\frac{\partial \overline{w}}{\partial \overline{x}}\right)^2 + \nu\left(\frac{\partial \overline{w}}{\partial \overline{y}}\right)^2\right)\left(\frac{\partial^2 \overline{w}}{\partial \overline{x}^2} + \frac{\partial^2 \overline{w}}{\partial \overline{y}^2}\right) - S_0 B_0^2\frac{\partial^2 \overline{w}}{\partial \overline{y}^2} + \quad (30)$$
$$2R_0\frac{\partial^2 \overline{w}}{\partial \overline{x}\partial \overline{y}}\frac{\partial \overline{w}}{\partial \overline{x}}\frac{\partial \overline{w}}{\partial \overline{y}} + \left(1-\mu\nabla^2\right)B_0^2\left[S_1\left(\frac{\partial \overline{w}}{\partial \overline{x}}\right)^2 + S_2\frac{\partial \overline{w}}{\partial \overline{x}}\right]$$
$$-2\left(1-\mu\nabla^2\right)S_0 B_0^2\left(\frac{\partial \overline{w}}{\partial \overline{y}}\right)^2 + \overline{P}_0 \sin \Omega\tau$$

In the following, for abbreviation, the superscript on the variables is ignored.

Solving the equations

Applying the Galerkin method

The Galerkin method is used to find the approximate solution of differential equations whose exact solution cannot be calculated [42-44]. In this method, the transverse displacement of graphene nanosheets is considered as follows:

$$w(x,y,\tau)=\sum_{m=1}^{\infty}\sum_{n=1}^{\infty}A_{mn}X_m(x)Y_n(y)\eta_{mn}(\tau) \quad (31)$$

in which $X_m(x)$ and $Y_n(y)$ are the vibration mode shapes of the nanosheet. A_{mn} is the unknown constant of amplitude coefficient and $\eta_{mn}(\tau)$ is the response of the time part. In this study, three types of boundary conditions are used for the analysis. These boundary conditions are:

The first boundary condition: All the edges of the nanosheets are simply supported (SSSS).

$$X_m=\sin(m\pi x) \quad (32)$$

$$Y_n=\sin(n\pi y) \quad (33)$$

The second boundary condition: the two opposite edges are simply supported and the other two edges are clamped (SCSC).

$$X_m=\sin(m\pi x) \quad (34)$$

$$Y_n=(\cosh(\lambda_n y)-\cos(\lambda_n y)-a_n\left[\sinh(\lambda_n y)-\sin(\lambda_n y)\right]) \quad (35)$$

Third boundary condition: all edges are clamped (CCCC)

$$X_m=(\cosh(\lambda_m x)-\cos(\lambda_m x)-a_m\left[\sinh(\lambda_m x)-\sin(\lambda_m x)\right]) \quad (36)$$

$$Y_n=(\cosh(\lambda_n y)-\cos(\lambda_n y)-a_n\left[\sinh(\lambda_n y)-\sin(\lambda_n y)\right]) \quad (37)$$

Which in relations (36) - (38), λ_m, λ_n, a_m and a_n constants, are obtained using the method proposed in Ref. [45]. By placing the hypothetical answer of Eq. (32) in the equation of motion (31), and by multiplying the sides of the above equation by X_mY_n and integrating on the nanosheet surface, the equation of motion was obtained as the following form:

$$M\ddot{\eta}+K\eta+\xi C\dot{\eta}+B_0^2N\eta^2+G\eta^3=P\sin\Omega\tau \quad (38)$$

where

$$M=\int_0^1\int_0^1\left(X_1Y_1-\mu^2\left(X_1''Y_1+X_1Y_1''\right)\right)X_1Y_1dxdy \quad (39)$$

$$K=\int_0^1\int_0^1\Big[\left(X_1''Y_1''+\nu X_1^{(4)}\ Y_1\right)+\left(X_1Y_1''''+\nu X_1''Y_1\right)+\left(X_1Y_1^{(4)}+\nu X_1''Y_1''\right)+S_0B_0^2X_1Y''\Big]X_1Y_1dxdy \quad (40)$$

$$C=\int_0^1\int_0^1\left(X_1Y_1\right)^2dxdy \quad (41)$$

$$N=\int_0^1\int_0^1\left(1-\mu\nabla^2\right)\Big(S_1\left(X_1'Y_1\right)^2-2S_0\left(\left(X_1Y_1'\right)^2+\left(X_1'Y_1\right)^2\right)\Big)X_1Y_1dxdy \quad (42)$$

Solve using the multiple time scales method

In order to use the multiple time scales method, by dividing the sides of Eq. (38) by M and using variable change of $\eta=\varepsilon\psi$ and assuming the order of $\xi\bar{C}\dot{\eta}$ is equal $2\varepsilon^2\xi\bar{C}\dot{\eta}$ and $\bar{P}\sin\Omega\tau$ is equal $\varepsilon^3\bar{P}\sin\Omega\tau$, we would have:

$$\ddot{\psi}+\omega^2\psi=-2\varepsilon^2\xi\bar{C}\dot{\psi}-\varepsilon B_0^2\bar{N}\psi^2-\varepsilon^2\bar{G}\psi^3+\varepsilon^2\bar{P}\sin\Omega\tau \quad (44)$$

where $\omega_0=\sqrt{K/M}$ is the frequency of the corresponding linear system and the – sign indicates the division of the variable by M.

To use the multiple time scales method, the answer of Eq. (45) is considered as follows [35]:

$$\psi\left(\tau,\varepsilon,T_2\right)=\psi_0\left(T_0,T_1,T_2\right)+\varepsilon\psi_1\left(T_0,T_1,T_2\right)+O(\varepsilon^2) \quad (45)$$

where $T_0=\tau$ represents fast time and $T_1=\varepsilon\tau$ and $T_2=\varepsilon^2\tau$ is the slow time. Therefore, the first and second derivatives can be expressed as follows:

$$\frac{d}{d\tau}=D_0+\varepsilon D_1+\varepsilon^2D_2,\ \frac{d^2}{d\tau^2}=D_0^2+2\varepsilon D_0D_1+\varepsilon^2\left(D_1^2+2D_0D_2\right) \quad (46)$$

To investigate the response around the initial resonance, the parameter σ is defined considering the excitation frequency Ω around

the natural frequency ω_0 according to Eq. (47).

$$\Omega = \omega_0 + \varepsilon^2 \sigma \tag{47}$$

Substituting Eqs. (45) and (46) and using Eq. (47) and unifying coefficients of different powers of ε in both sides, the equations are obtained as:

$$D_0^2\psi_0 + \omega_0^2\psi_0 = 0 \tag{48}$$

$$D_0^2\psi_1 + \omega_0^2\psi_1 = -2D_0D_1\psi_0 - B_0^2\overline{N}\psi_0^2 \tag{49}$$

$$\begin{aligned} D_0^2\psi_2 + \omega_0^2\psi_2 &= -2D_0D_1\psi_1 - 2D_0D_2\psi_0 - 2\xi\overline{C}D_0\psi_0 \\ &\quad - 2B_0^2\overline{N}\psi_0\psi_1 - \overline{G}\psi_0^3 + \overline{P}\sin\left(\omega_0T_0 + \sigma T_2\right) \end{aligned} \tag{50}$$

where the general answer of Eq. (48) can be written as:

$$\psi_0 = A(T_1, T_2)\exp(i\omega_0T_0) + \overline{A}(T_1, T_2)\exp(-i\omega_0T_0) \tag{51}$$

By placing ψ_0 in Eq. (49) one would have:

$$\begin{aligned} D_0^2\psi_1 + \omega_0^2\psi_1 &= -2i\omega_0D_1A\exp(i\omega_0T_0) - \\ B_0^2\overline{N}&\left[A^2\exp(2i\omega_0T_0) + A\overline{A}\right] \end{aligned} \tag{52}$$

By removing the secular terms [46] in relation (52), one would have $D_1A = 0$ which shows $A = A(T_2)$. Therefore, the solution of Eq. (48) would be as:

$$\psi_1 = \frac{B_0^2\overline{N}}{\omega_0^2}\left[-2A\overline{A} + \frac{1}{3}A^2\exp(2i\omega_0T_0) + \frac{1}{3}\overline{A}^2\exp(-2i\omega_0T_0)\right] \tag{53}$$

By substituting ψ_0 and ψ_1 in Eq. (50) we will have:

$$\begin{aligned} D_0^2\psi_2 + \omega_0^2\psi_2 = -\Bigg[&2i\omega_0(A' + \xi\overline{C}A) + \left(3\overline{G} - \frac{10\left(B_0^2\overline{N}\right)^2}{3\omega_0^2}\right)A^2\overline{A} \\ &-\frac{1}{2}\overline{P}\exp(i\sigma T_2)\Bigg]\exp(i\omega_0T_0) + cc + NST \end{aligned} \tag{54}$$

where the prime represents the derivative with respect to T_2 and the NST represents the terms corresponding to $\exp(\pm 3i\omega_{mn}T_0)$. To remove secular sentences from the above relation you the following relation can be used:

$$2i\omega_o(A' + \xi\overline{C}A) + \left(3\overline{G} - \frac{10\left(B_0^2\overline{N}\right)^2}{3\omega_0^2}\right) \tag{55}$$

$$A^2\overline{A} - \frac{1}{2}\overline{P}\exp(i\sigma T_2) = 0$$

To solve the above equation, $A = \frac{1}{2}a\exp(i\lambda)$. By placing this relation in Eq. (55) and separating the real and imaginary parts, one would have:

$$a' = -\xi\overline{C}a + \frac{\overline{P}}{2\omega_0}\sin\gamma \tag{56}$$

$$a\lambda' = \frac{9\overline{G}\omega_0^2 - 10\left(B_0^2\overline{N}\right)^2}{24\omega_0^3}a^3 - \frac{\overline{P}}{2\omega_0}\cos\gamma \tag{57}$$

where:

$$\gamma = \sigma T_2 - \lambda \tag{58}$$

By removing λ from relations (56) and (57) we will have:

$$a\gamma' = a\sigma - \frac{9\overline{G}\omega_0^2 - 10\left(B_0^2\overline{N}\right)^2}{24\omega_0^3}a^3 + \frac{\overline{P}}{2\omega_0}\cos\gamma \tag{59}$$

In order to calculate the steady-state motion response, it is assumed that $a' = \gamma' = 0$. In this case, the unknowns a and γ which are the answers to Eqs. (56) and (59) can be obtained as follows:

$$\left(\xi\overline{C}\right)^2a^2 + \left(a\sigma - \frac{9\overline{G}\omega_0^2 - 10\left(B_0^2\overline{N}\right)^2}{24\omega_0^3}a^3\right)^2 = \frac{\overline{P}}{4\omega_0^2} \tag{60}$$

$$\tan\gamma = \frac{\xi\overline{C}}{\frac{9\overline{G}\omega_0^2 - 10\left(B_0^2\overline{N}\right)^2}{24\omega_0^3}\left(a^2 - \sigma\right)} \tag{61}$$

The parameter α is defined as $\alpha = (9\bar{G}\omega_0^2 - 10(B_0^2\bar{N})^2)/24\omega^3$ [46]. When $\alpha > 0$ nonlinearity will have a hardening effect and for $\alpha < 0$ nonlinearity will have a softening effect. Besides, for $\alpha = 0$ nonlinear behavior would be disappeared. Equation (60) is an implicit equation between parameters a and σ, and the amplitude of the excitation force, by which the curve of the frequency response function can be plotted. Finally, the second-order approximation response of the graphene vibrations in the magnetic field is obtained as follows:

$$\psi = a\cos(\omega_0\tau + \lambda) + \frac{1}{6}\frac{\varepsilon B_0^2\bar{N}}{\omega_0^2}a^2\cos(2\omega_0\tau + 2\lambda) + O(\varepsilon^2) \quad (62)$$

where a and γ are obtained using equations (60) and (61).

RESULTS AND DISCUSSIONS

In this section, numerical results for graphene nanosheets located in a magnetic field for three different boundary conditions including SSSS, SCSC and CCCC are presented. The mechanical properties of graphene nanosheets are considered as Young's modulus $E = 1.02\,\mathrm{TPa}$, density $\rho = 2300\,\mathrm{kg/m^3}$, thickness $h = 0.335\,\mathrm{nm}$, and Poisson's ratio $\nu = 0.36$ [47]. In addition, the electrical characteristics are considered as magnetic constant $\chi_m = 1.5\,\mathrm{T}$ and $\mu_0 = 4\pi\times10^{-7}\ \mathrm{N/A^2}$ [48].

Validation

By considering linear terms and ignoring nonlinear terms from the nanosheet equations of motion, the linear natural frequencies of the system can be obtained. In Table 1, the obtained natural frequencies obtained by the local and nonlocal models for square graphene are compared with the results of Ref. [49]. According to this table, it can be seen that the obtained results are completely consistent with the results of Ref. [49] and this shows the high accuracy of the present method. Also, in Table 2, the natural frequency of a simply supported single layer graphene nanosheet (E = 1.02TPa, h = 0.34 nm, ρ = 2300 kg / m^3, $l_x = l_y$ = 10 nm) have been compared with the exact solution results presented in Refs. [50] and [51]. As it can be seen, the numerical results obtained here have an acceptable consistency with the results of the exact solution.

Linear vibrations

First, linear vibration analyzes are performed on square graphene nanosheets and the effects of boundary conditions and small size parameter on the first non-dimensional natural frequency of square graphene nanosheets are considered. Tables 3-5 show the effect of magnetic field intensity and small size parameters on the first non-dimensional natural frequency of graphene nanosheets under SSSS, CCCC, and SCSC boundary

Table 1. Validation of the frequency ratios of square nanosheet.

μ	$\omega_1^{non}/\omega_1^{loc}$	
	Ref. [49]	Present results
0	1.0000	0.9999
0.5	0.9762	0.9762
1.0	0.9139	0.9139
1.5	0.8321	0.8321
2	0.7574	0.7574

Table 2. Comparison of the natural frequency of a single layer graphene nanosheet with SSSS boundary conditions.

	μ=0			μ=1	
	Present result	Exact[a]	Exact[b]	Present result	Exact[b]
ω_1 (THz)	10.5546	10.5586	10.5586	9.67153	9.67400
ω_2 (THz)	26.4761	26.4753	26.4753	21.6223	21.6246
ω_3 (THz)	52.7283	52.7295	52.7295	37.4056	37.4075

[a] $\omega = \sqrt{\frac{D}{\rho h}}\left[\left(\frac{m\pi}{a}\right)^2 + \left(\frac{n\pi}{b}\right)^2\right]$, taken from Ref. [51]

[b] $\omega = \sqrt{\frac{D}{\left(\rho h + \frac{1}{12}\rho h^3\left[(m\pi/a)^2 + (n\pi/b)^2\right]\right)\left(1 + \mu\left[(m\pi/a)^2 + (n\pi/b)^2\right]\right)}}\left[\left(\frac{m\pi}{a}\right)^2 + \left(\frac{n\pi}{b}\right)^2\right]$, taken from Ref. [50]

Table 3. The non-dimensional natural frequency of the graphene nanosheet with SSSS Boundary conditions.

Magnetic field (B_0)	nonlocal parameter (μ)				
	0	0.1	0.2	0.4	0.5
0	19.7391	17.1808	13.0726	7.97991	6.57947
5	19.6709	17.1214	13.0274	7.95175	6.55270
10	19.4685	16.9421	12.8951	7.86825	6.48835
20	18.6182	16.2085	12.3302	7.52595	6.20605
30	17.1174	14.8958	11.3364	6.91779	5.70465
40	14.7528	12.8406	9.77025	5.96345	4.91758
50	10.9953	9.57082	7.28180	4.44458	3.66516
60	1.62822	1.41718	1.07832	0.65817	0.54274

Table 4. The non-dimensional natural frequency of the graphene nanosheet with CCCC Boundary conditions.

Magnetic field (B_0)	nonlocal parameter (μ)				
	0	0.1	0.2	0.4	0.5
0	36.6299	35.1807	31.6867	23.9183	20.7973
5	36.5799	35.1327	31.6435	23.8857	20.7689
10	36.4292	34.9388	31.5132	23.7874	20.6834
20	35.8205	34.4033	30.9866	23.3899	20.3377
30	34.7822	33.4061	30.0884	22.7119	19.7482
40	33.2743	31.9578	28.7839	21.7272	18.8692
50	31.2287	29.9931	27.0143	20.3915	17.7306
60	28.5299	27.4011	24.6797	18.6292	16.1983
70	24.9767	23.9793	21.5978	16.3029	14.1755
80	20.0857	19.2911	17.3752	13.1154	11.4504
90	12.4175	11.9263	10.7418	8.10832	7.05027

Table 5. The non-dimensional natural frequency of the graphene nanosheet with SCSC Boundary conditions.

Magnetic field (B_0)	nonlocal parameter (μ)				
	0	0.1	0.2	0.4	0.5
0	29.0801	26.8612	22.2684	14.8759	12.5043
5	29.0258	26.7619	22.2268	14.8481	12.4809
10	28.8623	26.6112	22.1016	14.7645	12.4106
20	28.1989	25.9995	21.5936	14.4251	12.1253
30	27.0357	24.9467	20.7192	13.8541	11.6343
40	25.3721	23.3933	19.4229	12.9791	10.9099
50	23.0255	21.2297	17.6321	11.7787	9.90084
60	19.7829	18.5624	15.1559	10.1682	8.50657
70	15.0771	13.9012	11.5454	7.71263	6.48305
80	6.16713	5.68614	4.72254	3.15479	2.65183

conditions. As it can be seen, generally, by increasing the small size parameter and magnetic field intensity, the natural frequency decreases and the quantity of this decrease depends on the boundary conditions. For example, for the nanosheet under the SSSS boundary condition, $\mu = 0.1$ increasing B_0 from 0 to 50, would result in decreasing the first natural frequency from 17.18 Hz to 9.57 Hz, which indicates a decrease of about 44% in the first natural frequency. Hence, it can be concluded that the intensity of the magnetic field has a significant effect on reducing the equivalent stiffness of the structure and consequently the vibration characteristics of the nanosheets. In addition, the nonlocal parameter reduces the equivalent stiffness of nanosheets. For SSSS nanosheet and for $B_0 = 20$, the natural frequency decreases by about 67% by increasing μ from 0 to 0.5.

Figs. 4 to 6 show the effect of magnetic field intensity and nonlocal parameters on the natural frequency of graphene nanosheet with SSSS, CCCC, and SCSC boundary conditions, respectively. These results also show that increasing the intensity of the magnetic field reduces the natural frequency. According to Eq. (31), the magnetic field has two different effects on the nanosheet: first, it reduces the flexural stiffness of the nanosheet,

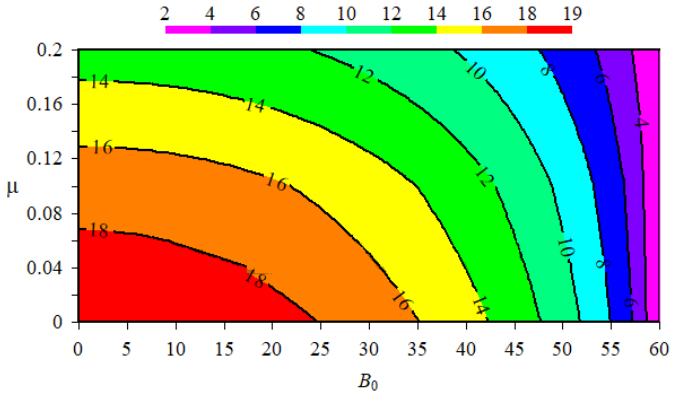

Fig. 4. Effect of magnetic field intensity and nonlocal parameter on the natural frequency of graphene nanosheet with SSSS boundary conditions.

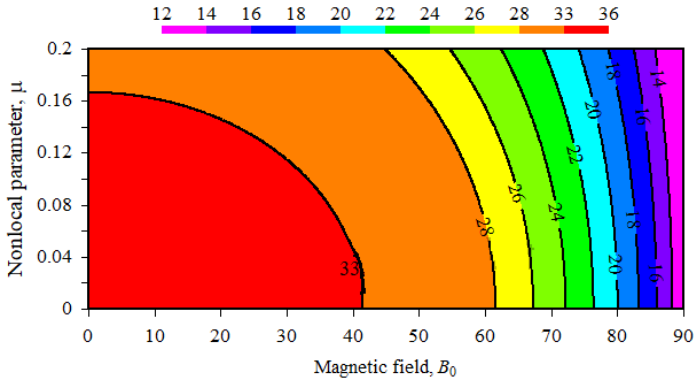

Fig. 5. Effect of magnetic field intensity and nonlocal parameter on the natural frequency of graphene nanosheet with SCSC boundary conditions.

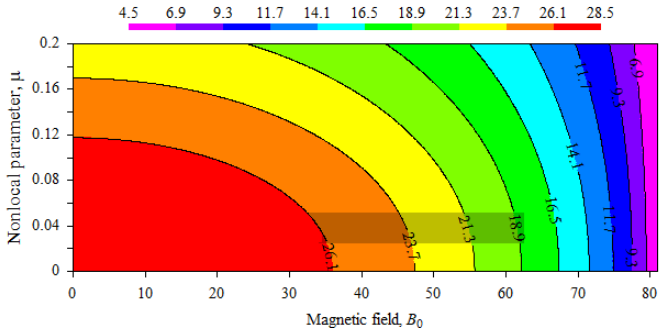

Fig. 6. Effect of magnetic field intensity and nonlocal parameter on the natural frequency of graphene nanosheet with CCCC boundary conditions.

and second, it applies an in-plane compressive force on the nanosheet. This effect reduces the flexural stiffness of the graphene nanosheet and thus reduces its natural frequency, which can be seen in Fig. 4. In addition, it is observed that the decreasing effect of the magnetic field on the natural frequency also depends on the boundary conditions. The maximum reduction of the natural frequency is seen for the SSSS nanosheet. Given that the magnetic field reduces the natural frequency of the system, it can be said that the magnetic field causes a softening behavior and therefore, excessive increase of the magnetic field can cause instability in the system.

As previously concluded, the magnetic field generates an in-plane compressive force. Hence,

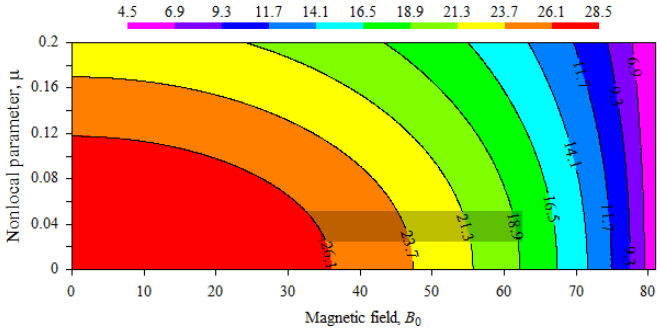

Fig. 7. Effect of the magnetic field intensity on the first natural frequency of the graphene nanosheet for the (a) SSSS, (b) CCCC, and (c) SCSC boundary conditions.

it is expected that for a certain amount of this force, static instability will occur in the system and the nanosheet will undergo static buckling**.** Figs. 7a, 7b, and 7c show the effect of magnetic field intensity on the first natural frequency of the SSSS, CCCC, and SCSC graphene nanosheets, respectively. According to the fig., it is observed that an increase B_0 would result in decreasing the first natural frequency till for the critical magnetic field B_0^{cr}, the first natural frequency becomes zero. For this amount of magnetic field, static buckling occurs in the system. Based on the results of Figs. 7a, 7b, and 7c, it can be seen that B_0^{cr} is highly dependent on the type of boundary conditions. For example for $\mu = 0$ when the nanosheet is under the SSSS, CCCC, and SCSC boundary conditions, it is obtained as 33.6, 95.1, and 72.3, respectively. As expected, the critical magnetic field increases for the clamped boundary conditions by increasing the stiffness of the nanosheet boundary conditions. In addition, it is observed that by increasing the nonlocal parameter, the natural frequency decreases and as a result, the critical magnetic field decreases. The main effect of the nonlocal parameter is observed for the SSSS boundary conditions. An interesting result that is observed for all boundary conditions is that for the values of the critical magnetic field, the nonlocal parameter does not affect and the value of the critical magnetic field is independent of this parameter. The examination of the results shows that the small size parameter reduces the natural frequencies, and this decrease in frequency is due to the decrease in the equivalent stiffness of the structure with the increase of this parameter. Moreover, the equivalent stiffness, which changes by the small size parameter, is zero at the critical buckling point. Accordingly, the small size parameter has no effect on the critical buckling load due the magnetic field. In other words, the natural frequency or the equivalent stiffness is zero at the critical buckling point, so the effect of the small size parameter is neglected on the critical buckling load.

Frequency amplitude curves

Frequency curves for graphene nanosheets located in the magnetic field can be calculated for all boundary conditions using Eq. (61). First, the changes of the frequency function curve for different values of magnetic field intensity are investigated. Fig. 8-10 show the frequency function curves for different values of and three different boundary conditions SSSS, CCCC, and SCSC. As can be seen in Fig. 8 (SSSS nanosheet), by increasing the intensity of the magnetic field, the amplitude curve bends to the left side, which indicates the softening behavior of the hard spring as a result of the reduction of the equivalent stiffness of the structure. In this case, the value of the parameter α in Eq. (61), which is negative, increases, and hence its value becomes positive for the values B_0 greater than 30. A similar situation is seen for the CCCC nanosheets (Fig. 9). In this case, as the magnetic field increases, the amplitude curve bends to the left side, which indicates the softening behavior of the hardening spring. Again the parameter α is negative, and as the magnetic field increases, its value tends to be positive. According to Fig. 10, similar behavior is observed for the SCSC nanosheet.

Another important parameter on the vibration behavior of nanosheets is the effect of small sizes parameter. The effect of small sizes on the amplitude curve of the nanosheet located in the magnetic field is shown in Figs. 11-13. According

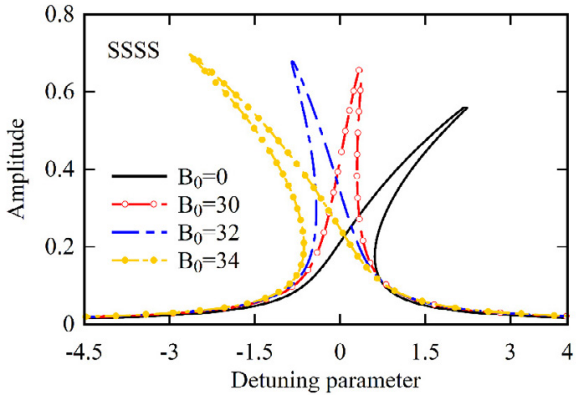

Fig. 8. Effect of magnetic field intensity on the frequency curve of graphene nanosheet for SSSS boundary conditions.

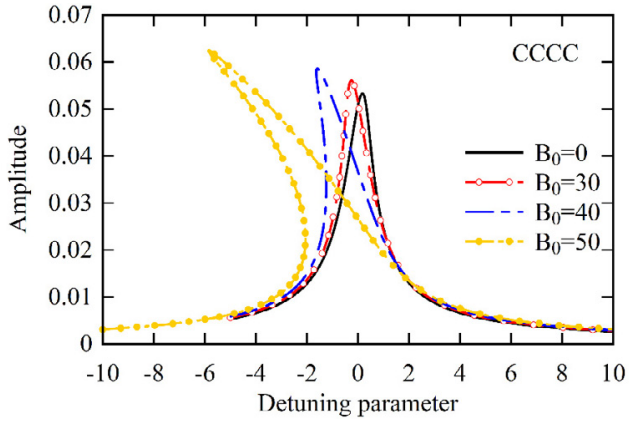

Fig. 9. Effect of magnetic field intensity on the frequency curve of graphene nanosheet for CCCC boundary conditions.

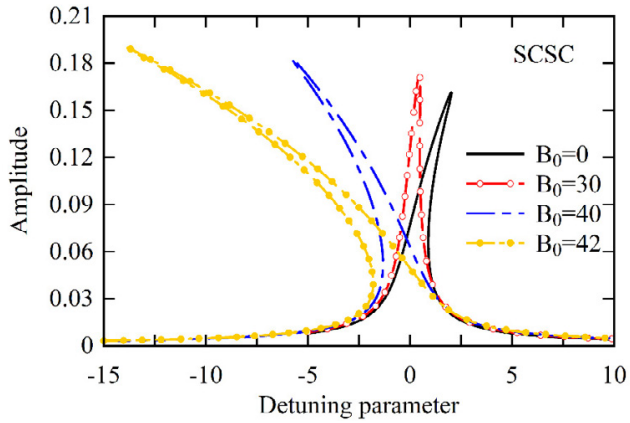

Fig. 10. Effect of magnetic field intensity on the frequency curve of graphene nanosheet for SCSC boundary conditions.

to the results, it can be seen that for all three considered boundary conditions, the increasing μ leads to enhance in the hardening behavior, which is more significant for SSSS nanosheets. The results show that for the CCCC boundary conditions (Fig. 11) by increasing μ, the value of the α parameter decreases and approaches zero, which causes the softening behavior of the hard spring. An opposite behavior is seen for SSSS (Fig. 12) and SCSC (Fig. 13) boundary conditions. Therefore, it can be said that in the graphene nanosheets, the nonlocal parameter is one of the most influential

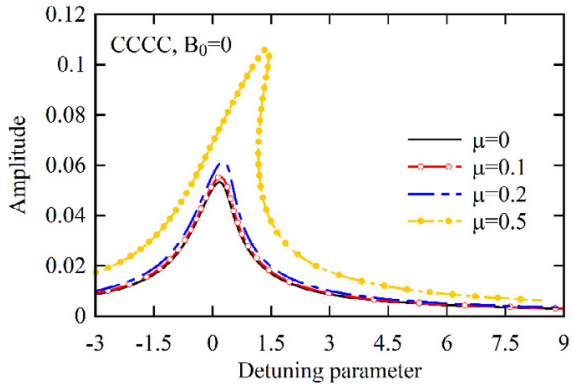

Fig. 11. Effect of nonlocal parameter on graphene nanosheet frequency curve for CCCC boundary conditions.

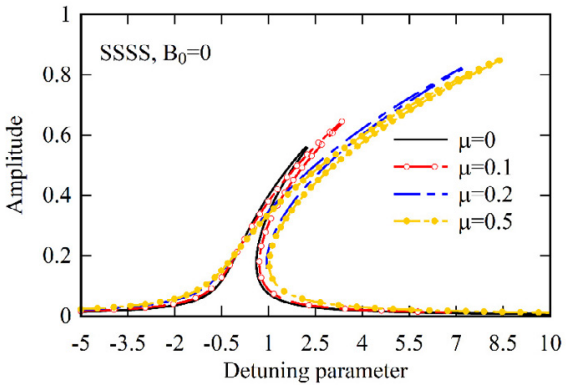

Fig. 12. Effect of nonlocal parameter on graphene nanosheet frequency curve for SSSS boundary conditions.

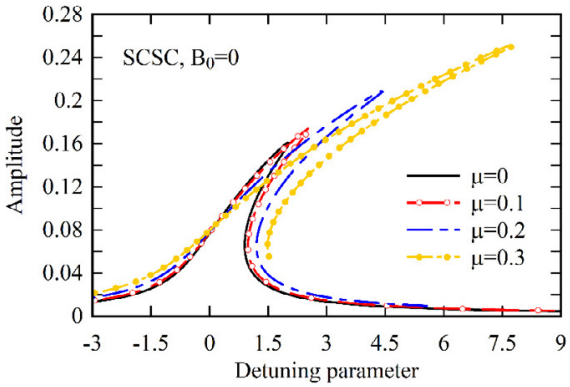

Fig. 13. Effect of nonlocal parameter on graphene nanosheet frequency curve for SCSC boundary conditions.

parameters on their dynamic behavior. Since the use of nonlocal theories in the study of the dynamic behavior of graphene nanosheets is practically inevitable, so in the design and analysis of such systems, the effect of nonlocal theories and nonlocal parameters should be considered.

In order to evaluate the accuracy and convergence of the proposed analytical method, Eq. (44) is numerically solved using the Rang-Kutta method and the results are compared with the time response obtained from the analytical solution (Eq. 62) in Fig. 14. As can be seen, the multiple time scales method provides the solution of the nonlinear equation of motion with very good accuracy and the maximum error in calculating the maximum amplitude is about 6%.

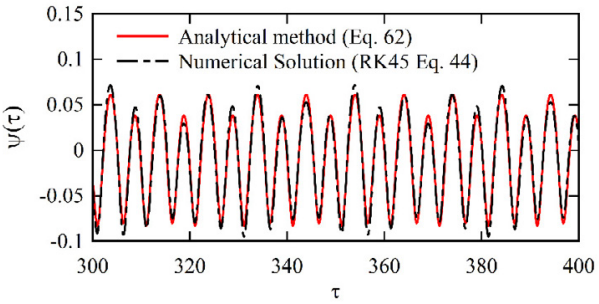

Fig. 14. Time response of the system obtained from analytical and numerical methods.

CONCLUSION

In this paper, based on the nonlocal elasticity theory, a new mathematical model was proposed to study the buckling behavior and nonlinear vibrations of graphene nanosheets located in a magnetic field. The effect of magnetic fields was applied to the equations by considering the additional flexural forces and moments created by the magnetic field. Analytical study of linear and nonlinear vibrations was performed for different boundary conditions. Besides, the effects of magnetic field intensity and nonlocal parameters on static buckling, vibrational frequency, and frequency response curve were studied. The results show:

- The nonlocal parameter reduces the equivalent stiffness of the nanosheets and as its value increases, the natural frequency decreases.

- Increasing the magnetic field, the first natural frequency decreases till for the critical magnetic field, the first natural frequency becomes zero and static buckling occurs in the system.

- It was observed that by increasing the intensity of the magnetic field, the amplitude curve bends to the left, which indicates the softening behavior of the hard spring as a result of reducing the rigidity equivalent to the structure.

- For all of the selected boundary conditions, increasing μ results in enhancing the hardening behavior, which is more pronounced for the SSSS nanosheets. For the CCCC boundary conditions, by increasing μ, the value of α decreases and approaches to zero. However, an opposite behavior is seen for SSSS and SCSC boundary conditions.

- It can be said that for the graphene nanosheets, the nonlocal parameter is one of the most influential parameters on dynamic behavior.

- An interesting result that is observed for all boundary conditions is that for the values of the critical magnetic field, the nonlocal parameter does not affect and the value of the critical magnetic field is independent of this parameter.

Hence, since the use of nonlocal theories in the study of the dynamic behavior of graphene nanosheets is practically inevitable, in the design and analysis of such systems, the effect of nonlocal theories and nonlocal parameters should be taken into account.

NOMENCLATURE

l	length
h	thickness
A_{mn}	unknown constant
B	magnetic field intensity
C	fourth-order elasticity tensor
c	structural damping
D	flexural stiffness
E	Young's modulus
F_z	external force
G	shear modulus
H	magnetic flux density
J	density-current vector
M_x, M_y, M_{xy}	resultant momentums
M	magnetization vector
N_x, N_y, N_{xy}	resultant forces
P_0	force amplitude
P_z	mechanical force
R_0, S_0, S_1	Nondimensional parameter
u_1, u_2	plane displacements
u_3, w	transverse displacement
ε	strain tensor
σ^{nl}	nonlocal stress tensor
μ	scale parameter

ν	Poisson's ratio
$\boldsymbol{\kappa}$	curvature vector
ω	force-frequency
Ω	Nondimensional frequency
τ	Nondimensional time

REFERENCES

[1] Nabavi M., Nazarpour V., Alibak A. H., Bagherzadeh A., Alizadeh S. M., (2021), Smart tracking of the influence of alumina nanoparticles on the thermal coefficient of nanosuspensions: Application of LS-SVM methodology. *App. Nano.* 34: 1-16.

[2] Kaabipour S., Hemmati S., (2021), A review on the green and sustainable synthesis of silver nanoparticles and one-dimensional silver nanostructures. *Beilstein J. Nanotechnol.* 12: 102-136.

[3] Seaberg J., Kaabipour S., Hemmati S., Ramsey J. D., (2020), A rapid millifluidic synthesis of tunable polymer-protein nanoparticles. *Eur. J. Pharm. Biopharm.* 154: 127-135.

[4] Biswas N., Sarkar U. K., Chamkha A. J.. Manna N. K., (2021), Magneto-hydrodynamic thermal convection of Cu–Al_2O_3/ water hybrid nanofluid saturated with porous media subjected to half-sinusoidal nonuniform heating. *J. Therm. Anal. Calorim*. 143: 1727-1753.

[5] Biswas N., Manna N. K., Chamkha A. J., (2021), Effects of half-sinusoidal nonuniform heating during MHD thermal convection in Cu–Al_2O_3/water hybrid nanofluid saturated with porous media. *J. Therm. Anal. Calorim.* 143: 1665-1688.

[6] Farzaneh A., Mohammadi M., Ahmad Z., Ahmad I., (2013), Aluminium alloys in solar power− Benefits and Limitations. Chapter 13.

[7] Farzaneh A., Esrafili M. D., Mermer Ö., (2020), Development of TiO_2 nanofibers based semiconducting humidity sensor: Adsorption kinetics and DFT computations. *Mater. Chem. Phys.* 239: 56-78.

[8] Farzaneh A., Mohammadzadeh A., Esrafili M.D., Mermer O., (2019), Experimental and theoretical study of TiO_2 based nanostructured semiconducting humidity sensor. *Ceram. Int.* 45: 8362-8369.

[9] Biswas N., Manna N. K., Datta P., Mahapatra P. S., (2018), Analysis of heat transfer and pumping power for bottom-heated porous cavity saturated with Cu-water nanofluid. *Powder Technol.* 326: 356-369.

[10] Nabavi M., Elveny M., Danshina S. D., Behroyan I., Babanezhad M., (2021), Velocity prediction of Cu/water nanofluid convective flow in a circular tube: Learning CFD data by differential evolution algorithm based fuzzy inference system (DEFIS). *Int. Commun. Heat Mass Transf.* 126: 34-56.

[11] Esmaeili J., Andalibi H., (2013), Investigation of the effects of nano-silica on the properties of concrete in comparison with micro-silica. *Int. J. Nano Dimens.* 3: 321-328.

[12] Pashaki V., Milad Pouya P., Maleki V. A., (2018), High-speed cryogenic machining of the carbon nanotube reinforced nanocomposites: Finite element analysis and simulation. *Proc. Inst. Mech. Eng. Mechan.* 232: 1927-1936.

[13] Rezaee M., Maleki V. A., (2015), An analytical solution for vibration analysis of carbon nanotube conveying viscose fluid embedded in visco-elastic medium. *Proc. Inst. Mech. Eng. Pt. Mechan.* 229: 644-650.

[14] Mondal M. K., Biswas N., Manna N. K., (2019), MHD convection in a partially driven cavity with corner heating. *SN App. Sci.* 1: 1-19.

[15] Manna N. K., Mondal M. K., Biswas N., (2021), A novel multi-banding application of magnetic field to convective transport system filled with porous medium and hybrid nanofluid. *Phy. Scripta*. 96: 56-78.

[16] Manna N. K., Biswas N., (2021), Magnetic force vectors as a new visualization tool for magnetohydrodynamic convection. *Int. J. Therm. Sci.* 167: 45-67.

[17] Ajri M., Rastgoo A., Fakhrabadi M. M. S., (2019), Non-stationary vibration and super-harmonic resonances of nonlinear viscoelastic nano-resonators. *Struc. Eng. Mech*. 70: 623–637.

[18] Tourki S. A., Hosseini Hashemi S., (2012), Buckling analysis of graphene nanosheets based on nonlocal elasticity theory. *Int. J. Nano Dimens*. 2: 227-232.

[19] Kaabipour S., Hemmati S., (2021), A review on the green and sustainable synthesis of silver nanoparticles and one-dimensional silver nanostructures. *Beilstein J. Nanotechnol.* 12: 102-136.

[20] Gao K., Gao W., Chen D., Yang J., (2018), Nonlinear free vibration of functionally graded graphene platelets reinforced porous nanocomposite plates resting on elastic foundation. *Comp. Struct*. 204: 831–846.

[21] Beitollai H., Safaei M., Tajik S., (2019), Application of Graphene and Graphene Oxide for modification of electrochemical sensors and biosensors: A review. *Int. J. Nano Dimens*. 10: 125-140.

[22] Aghababaei R., Reddy J. N., (2009), Nonlocal third-order shear deformation plate theory with application to bending and vibration of plates. *J. Sound. Vib.* 326: 277–289.

[23] Murmu T., Pradhan S. C., (2009), Vibration analysis of nano-single-layered graphene sheets embedded in elastic medium based on nonlocal elasticity theory. *J. Appl. Phy.* 105: 23-45.

[24] Ebrahimi F., Barati M. R., (2018), Vibration analysis of graphene sheets resting on the orthotropic elastic medium subjected to hygro-thermal and in-plane magnetic fields based on the nonlocal strain gradient theory. *Proc. Inst. Mech. Eng. Mech.* 232: 2469–2481.

[25] Jalaei M. H., Ghorbanpour-Arani A., (2018), Size-dependent static and dynamic responses of embedded double-layered graphene sheets under longitudinal magnetic field with arbitrary boundary conditions. *Comp. B. Eng*. 142: 117–130.

[26] Murmu T., McCarthy M. A., Adhikari S., (2013), In-plane magnetic field affected transverse vibration of embedded single-layer graphene sheets using equivalent nonlocal elasticity approach. *Compos. Struct*. 96: 57–63.

[27] Biglari A. E. H., (2017), Transverse vibration of single-layer graphene sheet under 2D magnetic field action by differential quadrature method. *Aerosp. Knwl. Sci. Technol. J*. 6: 81–92.

[28] Farajpour A., Mohammadi M., Shahidi A. R., Mahzoon M., (2011), Axisymmetric buckling of the circular graphene sheets with the nonlocal continuum plate model. *Phys. E. Low Dimens. Syst. Nanostruct*. 43: 1820–1825.

[29] Samaei A. T., Abbasion S., Mirsayar M. M., (2011), Buckling analysis of a single-layer graphene sheet embedded in an

elastic medium based on nonlocal Mindlin plate theory. *Mech. Res. Commun*. 38: 481–485.

[30] Pradhan S. C., (2009), Buckling of single layer graphene sheet based on nonlocal elasticity and higher order shear deformation theory. *Phys. Lett. A*. 373: 4182–4188.

[31] Allahyari E., Asgari M., Jafari A. A., (2020), Nonlinear size-dependent vibration behavior of graphene nanoplate considering surfaces effects using a multiple-scale technique. *Mech. Adv. Mat. Struc.* 27: 697-706.

[32] Rong D., Fan J., Lim C. W., Xu X., Zhou Z., (2018), A new analytical approach for free vibration, buckling and forced vibration of rectangular nanoplates based on nonlocal elasticity theory. *Int. J. Struct. Stab. Dyn*. 18: 1850055.

[33] Saadatmand M., Shahabodini A., Ahmadi B., Chegini S. N., (2021), Nonlinear forced vibrations of initially curved rectangular single layer graphene sheets: An analytical approach. *Phys. E: Low-Dimens. Syst. Nanostruc.* 127: 34-56.

[34] Mortazavi B., Cuniberti G., Rabczuk T., (2015), Mechanical properties and thermal conductivity of graphitic carbon nitride: A molecular dynamics study. *Comput. Mater. Sci.* 99: 285–289.

[35] Huang J., Ma Z., Wu Z., Peng L., Su B., (2021), Magnetic sensitive Crack sensor with ultrahigh sensitivity at room temperature by depositing graphene nanosheets upon a flexible magnetic film. *Adv. Elec. Mate.* 34: 56-67.

[36] Dhakal U., Rai D., (2019), Magnetic field control of current through model graphene nanosheets. *Phy. Lett. A*. 383: 2193-2200.

[37] Terdalkar S. S., Huang S., Yuan H., Rencis J. J., Zhu T., Zhang S., (2010), Nanoscale fracture in graphene. *Chem. Phys. Lett*. 494: 218–222.

[38] Ismail R., Cartmell M. P., (2012), An investigation into the vibration analysis of a plate with a surface crack of variable angular orientation. *J. Sound. Vib.* 331: 2929–2948.

[39] Joshi P. V., Jain N. K., Ramtekkar G. D., (2015), Analytical modelling for vibration analysis of partially cracked orthotropic rectangular plates. *Eur. J. Mech. A-Solids*. 50: 100–111.

[40] Israr A., Cartmell M. P., Manoach E., Trendafilova I., Ostachowicz W., Krawczuk M., Zak A., (2009), Analytical modeling and vibration analysis of partially cracked rectangular plates with different boundary conditions and loading. *J. Appl. Mech*. 76: 45-67.

[41] Pourreza T., Alijani A., Maleki V. A., Kazemi A., (2021), Nonlinear vibration of nanosheets subjected to electromagnetic fields and electrical current. *Techno-Press*. 10: 481–491.

[42] Ajri M., Rastgoo A., Fakhrabadi, M. M. S., (2020), How does flexoelectricity affect static bending and nonlinear dynamic response of nanoscale lipid bilayers? *Phys. Scr*. 95: 025001.

[43] Ghaderi M., Ghaffarzadeh H., A Maleki V., (2015), Investigation of the stability and vibration of cracked columns under compressive axial Load. *J. Ferdowsi. Civ. Eng.* 26: 21-23.

[44] Jahanghiry R., Yahyazadeh R., Sharafkhani N., Maleki V. A., (2016), Stability analysis of FGM microgripper subjected to nonlinear electrostatic and temperature variation loadings. *Sci. Eng. Compos. Mater.* 23: 199–207.

[45] Leissa A. W., (1969), Tabulated numerical results of theories of plate vibration. *Vibration of plates . NASA SP.* (patent No160).

[46] Nayfeh A. H., Mook D. T., Holmes P., (1980), Nonlinear oscillations. *J. Appl. Mech*. 47: 692-693.

[47] Cao G., (2014), Atomistic studies of mechanical properties of Graphene. *Polymers*. 6: 2404-2432.

[48] Mousavi H., Bagheri M., Khodadadi J., (2015), Magnetic susceptibility and heat capacity of graphene in two-band Harrison model. *Phys. E. Low Dimens. Syst. Nanostruc*t. 74: 135–139.

[49] Wang Y., Li F. M., Wang Y. Z., (2015), Nonlinear vibration of double layered viscoelastic nanoplates based on nonlocal theory. *Phys. E. Low Dimens. Syst. Nanostruc*t. 67: 65–76.

[50] Pradhan S. C., Phadikar J. K., (2009), Nonlocal elasticity theory for vibration of nanoplates. *J. Sound. Vib.* 325: 206–223.

[51] Kitipornchai S., He X. Q., Liew K. M., (2005), Continuum model for the vibration of multilayered graphene sheets. *Phys. Rev. B.* 72: 075443.